

# High-performance silicon carbide polarization beam splitting based on an asymmetric directional couplers for mode conversion

**Shi, Xiaodong; Lu, Yaoqin; Ou, Haiyan**

*Published in:*
Optics Letters

*Link to article, DOI:*
10.1364/OL.481314

*Publication date:*
2023

*Document Version*
Peer reviewed version

# High-performance silicon carbide polarization beam splitting based on the asymmetric directional coupler for mode conversion

XIAODONG SHI[1], YAOQIN LU[1], AND HAIYAN OU[1,*]

[1] Department of Electrical and Photonics Engineering, Technical University of Denmark, Kgs. Lyngby, 2800, Denmark.
[*] Corresponding author: haou@dtu.dk

Compiled December 22, 2022

**Polarization manipulation and management are important for 4H-silicon carbide (SiC) integrated photonics, as 4H-SiC has material-based birefringent properties. In this paper, we propose a low-birefringence polarization beam splitter (PBS) based on asymmetric directional coupler (ADC) mode converters with overall high performances. We numerically and experimentally demonstrate the ADC mode conversion based PBS on a 4H-SiC chip. The experimental results show that the device exhibits high transmittance of -0.6 dB and -1.3 dB for the transverse-electric (TE) and transverse-magnetic (TM) polarized light, respectively and broad operational bandwidth over 130 nm. The polarization extinction ratio of >25 dB and >17 dB covering the whole C band for the TE and TM polarized light, respectively, and an ultra-large polarization extinction ratio of >32 dB for both polarizations at around 1560 nm are achieved.** 

http://dx.doi.org/10.1364/ao.XX.XXXXXX

Silicon carbide (SiC), exhibiting superior physical properties, is one of the most widely used third-generation semiconductors [1]. Its wide bandgap, as well as high saturation velocity and large breakdown voltage, makes SiC an attractive candidate for power electronics[2]. The wide bandgap property of SiC also enables a wide window of optical transparency in a wavelength range from near ultraviolet to mid-infrared and an eradication of two-photon absorption at telecom wavelength, benefiting optical applications [3]. Meanwhile, thanks to its strong second- and third-order optical nonlinearities and material-based color centers, SiC also attracts a lot of attentions in nonlinear and quantum optics [4–6]. Therefore, SiC is regarded as a growing alternative to silicon based electronic and photonic components. In recent years, the ion-cut technique and the grinding-chemical mechanical polishing method facilitate high-quality 4H-SiC-on-insulator (SiCOI) stacks, and the advanced nanofabrication technologies promote the development of 4H-SiC integrated photonics [7–13].

Polarization manipulation is very important in both photonic integrated circuits and quantum photonic integrated circuits, which can be used for on-chip polarization-division multiplexing and polarization entanglement-enabled quantum key distribution [14–17]. Especially, for the 4H-SiCOI integrated platform, the polarization control is an essential issue. Because 4H-SiC is a uniaxial crystal, optical properties, including refractive index and nonlinear refractive index, are crystal-orientation dependent. As a result, light with different polarizations, propagating in 4H-SiC waveguides, also show different properties [18, 19]. The polarization beam splitter (PBS) is one of the important devices for polarization manipulation, which is able to split or combine light beams with different polarizations. The performances of PBSs are evaluated by transmission efficiency, operational bandwidth, and polarization extinction ratio [20]. Although plenty of high-performance PBSs have been demonstrated in the silicon photonic integrated platform [21], it is still challenging to achieve in the SiC photonic integrated platform. Compared to silicon, SiC has relatively lower refractive index, which results in low birefringence of the orthogonal polarizations in the waveguides with large dimensions [7]. As a result, it is not efficient to make low-birefringence beam splitting with conventional directional couplers. A novel vertical-dual-slot structure has been proposed to achieve low-birefringence beam splitting in the SiC integrated platform with a small footprint, but the polarization extinction ratio is not satisfactory [7]. Therefore, it remains a demanding challenge to achieve PBSs with overall good performances in the SiC integrated platform.

Directional couplers and asymmetric directional couplers (ADC) have been widely used for efficient power coupling [22], mode conversion [23], as well as polarization beam splitting especially in silicon integrated platforms. The scheme of the directional coupler, assisted by a bridged waveguide, has been demonstrated to achieve high polarization extinction ratio for polarization beam splitting [24]. By using thin silicon layer to have large birefringence for the two polarizations, a higher polarization extinction ratio can be achieved [25]. An alternative way to increase the polarization extinction ratio is to apply ADC, for the purpose of enlarging the phase mismatching of the mode coupling for the two polarizations [26], and it is also valid for thick silicon layer [27]. Similar designs have also been reported in low-refractive-index materials based integrated platforms, such as silicon nitride and lithium niobate, showing great advantages for low-birefringence beam splitting [28, 29].

In this letter, we apply a pair of mode converters, based on ADC, for the low-birefringence polarization beam splitting in the SiC integrated platform. One mode converter is used to convert the fundamental TM ($TM_0$) mode to the first-order TM ($TM_1$) mode, according to the phase matching between the two modes. At the same time, it can split the orthogonal polarizations, because the phase-matching

condition is not valid for the TE modes. A cascaded identical mode converter is directly connected to the first mode converter, in order to convert the $TM_1$ mode back to the $TM_0$ mode. More importantly, it can further eliminate the leakage of the TE mode from the first mode converter, so that the polarization extinction ratio can be largely increased. The device is numerically and experimentally demonstrated with high transmission efficiency, broad operational bandwidth, and large polarization extinction ratio in the SiC integrated platform, within a small footprint.

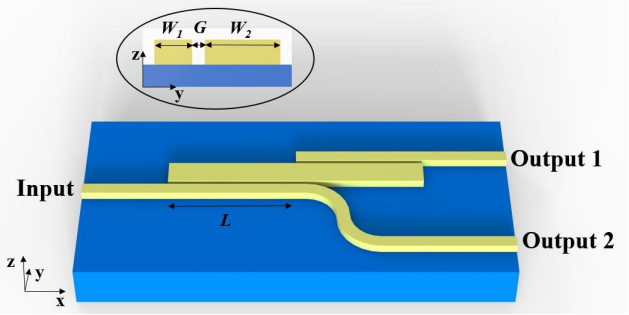


**Fig. 1.** Schematic of the ADC mode conversion based PBS.

Figure 1 shows the schematic of the proposed ADC mode conversion based PBS. The inset shows the cross section of an ADC mode converter. The device sits on a 4H-SiCOI integrated platform, with a 4H-SiC thin film thickness of 400 nm. The extraordinary optical axis of 4H-SiC is perpendicular to the wafer plane. The ADC mode converter consists of a single-mode waveguide and a multi-mode waveguide, with widths of $W_1$ and $W_2$, respectively. The coupling length and the gap between the two waveguides are $L$ and $G$, respectively. The two mode converters in the whole device have the same dimension. When light is injected from Input, after transmitting a pair of ADC mode converters, the TM-polarized light is coupled out to the upper waveguide at Output 1, while the TE-polarized light remains propagating in the same waveguide, and is coupled out at Output 2, with an S-bend waveguide.

In order to design efficient ADC mode converters, the waveguide widths are supposed to match the phase matching condition between the $TM_0$ and $TM_1$ modes, which means that the effective refractive index of the two modes are equivalent. We use Lumerical MODE Solutions to simulate the effective refractive index in 4H-SiC waveguides, and the anisotropic Sellmeier equation is applied to the refractive index of 4H-SiC material [18]. The effective refractive index, $n_{eff}$, of different guided modes is simulated with varying waveguide widths at the wavelength of $\lambda$ =1550 nm, as shown in Figure 2(a). The width of the input waveguide is selected to be $W_1$ =0.60 μm, which only confines the $TE_0$ and $TM_0$ modes. Then, the corresponding width of the multi-mode waveguide in the ADC mode converter should be $W_2 = 1.44$ μm, to satisfy the phase matching condition, given by $n_{eff,TM_0} = n_{eff,TM_1} = 1.78$, approximately.

After selecting the waveguide dimensions, we need to set the gap between the two waveguides in the ADC mode converter. The power coupling between the two waveguides in the ADC is jointly determined by the gap and the coupling length. The gap can influence the supermode distribution in the coupling region, as well as the coupling efficiency. The coupling length can be theoretically calculated through $L = \lambda / [2(n_{even} - n_{odd})]$, where $\lambda$ is the wavelength, $n_{even/odd}$ is the effective refractive index of the even/odd supermode in the ADC mode converter [30]. We find that as the gap is increasing, the effective refractive index difference between the even and the odd mode is reduced. Hence, the coupling length, which is inversely proportional

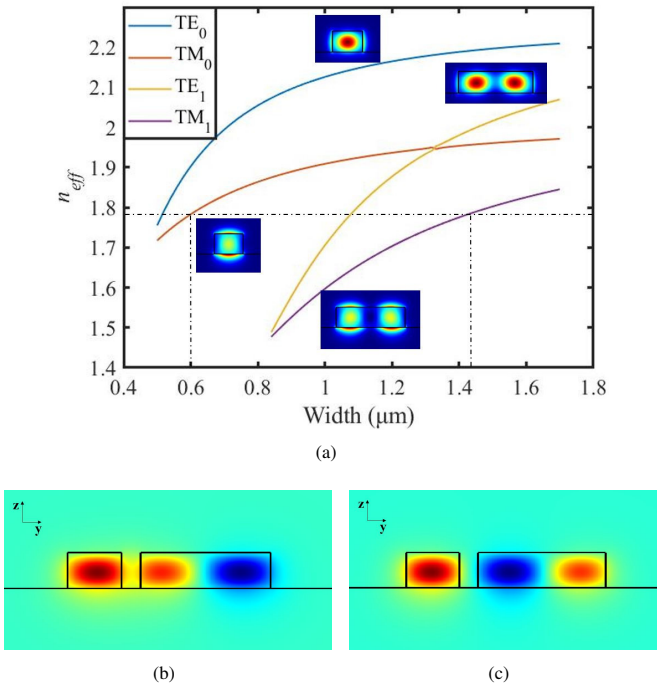


**Fig. 2.** (a) Effective refractive index of $TE_0$, $TE_1$, $TM_0$, $TM_1$ modes of 400 nm thick 4H-SiC waveguides as a function of the waveguide width, and the corresponding eigenmode profiles at 1550 nm. The magnetic-field profiles of (b) the even and (c) the odd TM supermodes in the coupling region.

to the effective refractive index difference, is increasing accordingly. Narrow gaps make efficient power coupling, but also require high nanofabrication resolution. Taking the trade-off between fabrication difficulty and the device compactness into consideration, we decide to choose the gap to be $G = 200$ nm. Figure 2(b) and 2(c) show the magnetic-field profiles of the even and the odd TM supermodes in the coupling region, respectively, with a gap of $G = 200$ nm. The effective refractive index of the even and the odd supermode is $n_{even} = 1.811$ and $n_{odd} = 1.763$, respectively. Thus, the coupling length is calculated to be 16 μm, when the wavelength is at $\lambda = 1550$ nm.

We also numerically simulate the coupling efficiency as a function of the coupling length, using Lumerical FDTD Solutions. The optimized coupling length is simulated to be $L = 14$ μm, considering a high transmittance of >-0.04 dB and a large polarization extinction ratio of >23 dB for both polarizations at the corresponding output, as shown in Figure 3(a) and 3(b). The polarization extinction ratio is defined by $PER_{\mathrm{TE}} = 10\log_{10}\frac{T_{\mathrm{TE_{Output2}}}}{T_{\mathrm{TE_{Output1}}}}$ and $PER_{\mathrm{TM}} = 10\log_{10}\frac{T_{\mathrm{TM_{Output1}}}}{T_{\mathrm{TM_{Output2}}}}$, for TE and TM polarized light, respectively, where $T$ is the transmission efficiency. The simulated coupling length is slightly shorter than the calculated one. It is because the start of the S-bend waveguide is still close to the multimode waveguide, and there could be some light coupling in that region.

We then simulate the transmission spectrum with the optimized PBS, as shown in Figure 3(c) and 3(d). At Output 1, the highest transmittance of the TM polarized light is >-0.04 dB with a wide 1 dB bandwidth of 190 nm from 1450 nm to 1640 nm. Thanks to the cascaded ADC mode converters, the TE polarized light leaks weakly at Output 1, <-20 dB. At Output 2, the TE polarized light also shows very high transmittance with an ultra wide 1 dB bandwidth of >300 nm. The polarization extinction ratio is plotted in Figure 3(e). The TE and TM polarized light shows high polarization extinction ratio of

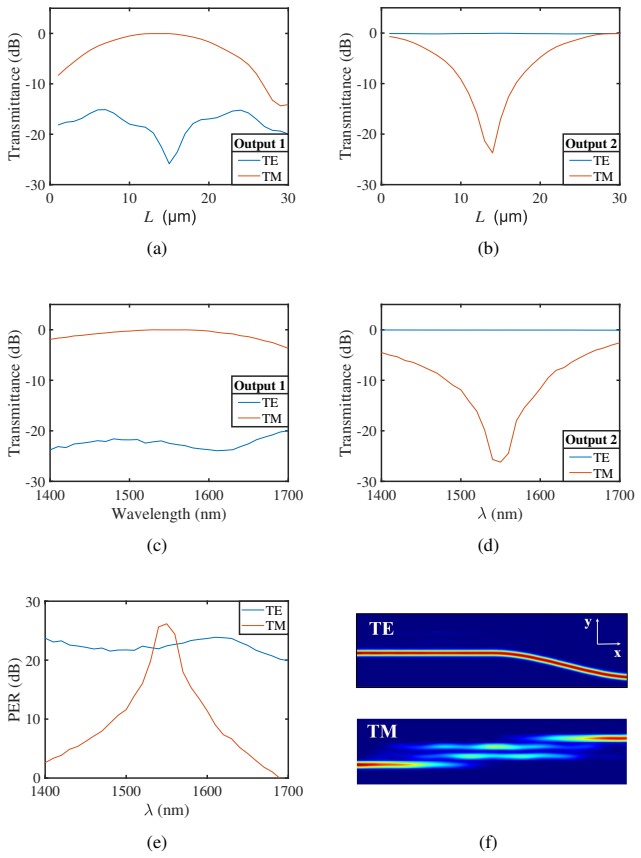


**Fig. 3.** Transmittance as a function of the coupling length at (a) Output 1 and (b) Output 2. Transmittance as a function of the wavelength at (c) Output 1 and (d) Output 2. (e) Polarization extinction ratio as a function of the wavelength. (f) Energy distribution of TE (upper) and (lower) TM polarized light in the PBS. It is noticed that the dimensions in x and y directions are not in scale.

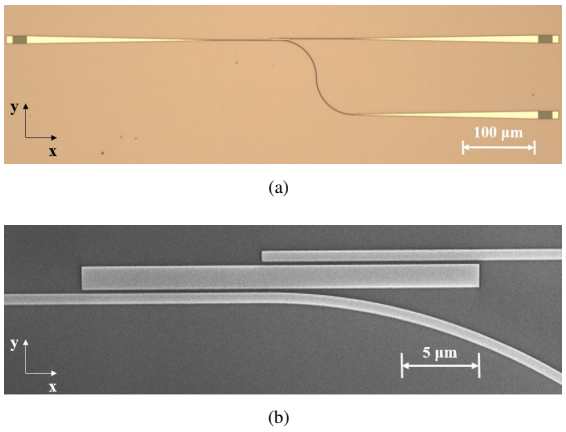


**Fig. 4.** (a) Microscope image of the ADC mode conversion based PBS with gratings at the input and output ports, fabricated in 4H-SiCOI integrated platform. (b) Zoom-in SEM image of the SiC ADC mode conversion based PBS.

>20 dB within a bandwidth of >300 nm and 40 nm from 1530 nm to 1570 nm, respectively. The device is sensitive to the wavelength for the TM polarization, due to the dispersion induced phase mismatching. Generally, from the simulation results, the proposed ADC mode conversion based PBS shows high efficiency, high polarization extinction ratio, and satisfactory operation bandwidth covering the whole C band. The energy distribution of the TE and TM polarized light in the device is shown in Figure 3(f). It is noticed that the energy distrubution in the central waveguide is not a perfect $TM_1$ mode, which is due to the multimode interference with the cross-coupled $TM_0$ mode [26]. All the parameters of the ADC mode conversion based PBS are summarized in Table 1.

**Table 1.** Optimized parameters of the ADC mode conversion based PBS.

| $W_1$ (μm) | $W_2$ (μm) | $G$ (nm) | $L$ (μm) |
|---|---|---|---|
| 0.6 | 1.44 | 200 | 14 |

After designing the PBS, we fabricate the device on a 4H-SiCOI chip, which is prepared through the ion-cut method [7]. The devices are patterned on the chip through electron-beam lithography and inductively coupled plasma-reactive ion etching [7]. Figure 4(a) shows the microscope image of the whole fabricated SiC testing device. The input and output ports are connected with polarization-insensitive grating couplers, which can couple light with both polarizations between the device and the fiber-based characterization system [19]. Figure 4(b) shows the scanning electron microscope (SEM) image of the fabricated SiC ADC mode converter based PBS.

We build the characterization setup, shown in Figure 5(a), to test the device. A tunable continuous-wave laser source (Santec TSL-510) launches light into a polarization controller. The polarized light is coupled in and out of the device through fibers and grating couplers. The output light is detected by a power meter (Santec MPM-212). The laser and the power meter are controlled by a computer for synchronized sweep to measure the transmission spectrum. Before the characterization, a microring resonator with resonances of both polarizations is used to calibrate the input polarization, according to the different free spectral ranges [19].

The normalized transmittance of the ADC mode conversion based PBS with both polarizations, measured from Output 1 and Output 2, is plotted in Figure 5(b) and 5(c), respectively. It is noticed that the normalized transmittance only shows the PBS performance, excluding the grating transmittance. As can be seen, the transmittance of the TM and TE polarized light at Output 1 and Output 2, respectively, is very high and flat, within the measured wavelength range between 1500 nm and 1630 nm. At Output 1, the highest transmittance of the TM polarized light is -1.3 dB at ∼1560 nm. It can be seen there are many ripples in the spectrum, that are deemed to be generated due to the interference in the ADC, as some light is reflected by the grating couplers. In spite of the ripples, the overall transmittance is >-3.3 dB over the whole measurement range. At Output 2, the highest transmittance of the TE polarized light is -0.6 dB, and the overall transmittance is >-1.5 dB over the whole measurement range, which means that the 1 dB transmission bandwidth is beyond 130 nm. The polarization extinction ratio as a function of the wavelength is plotted in Fig.5(d). It is seen that the polarization extinction ratio for the TM polarized light as high as 35 dB is achieved at ∼1560 nm, which is the phase matching wavelength. And it is >17 dB, between 1535 nm and 1595 nm, covering the whole C band and half L band. The polarization extinction ratio for the TE polarized light is also >30 dB at ∼1560 nm, and is >20 dB within the whole measured wavelength range. Such high

polarization extinction ratio is attributed to phase mismatching of the TE mode in the ADC, as well as the sidewall roughness induced light scattering in the coupling region, that results in weak cross coupling. It is seen that the simulation well predicts and guides to perform the experiment, and we acquire a PBS with overall good performances, except for a slight red shift of the spectrum. The phase matching wavelength is red shifted by ∼10 nm in the experiment, which could be due to the linewidth variation and fabrication imperfections in the fabrication processes. We find that a linewidth reduction of 10 nm can induce a red shift of the phase matching wavelength by ∼10 nm, from the simulation.

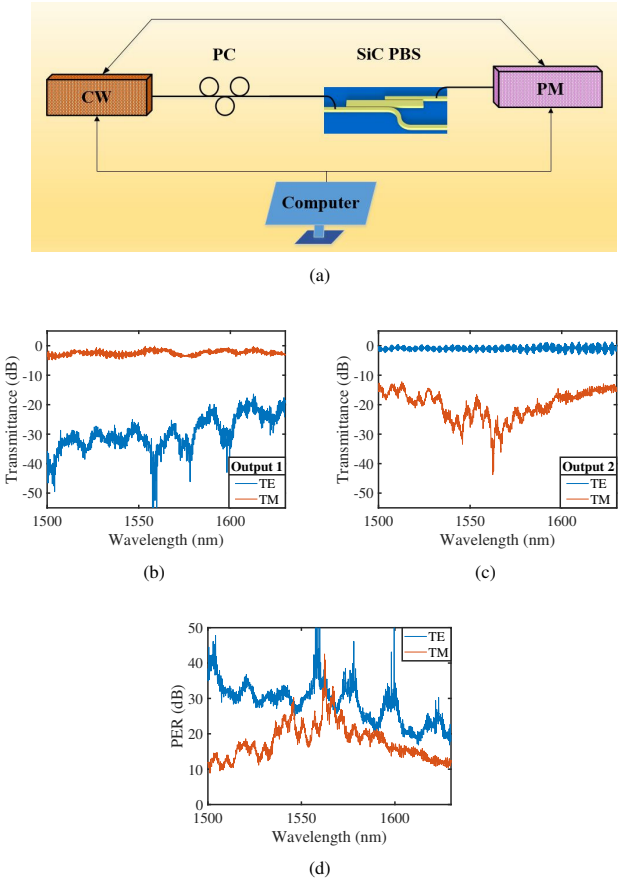


**Fig. 5.** (a) Measurement setup schematic, CW: tunable continuous-wave laser, PC: polarization controller, PM: power meter. The measured results of normalized transmittance at (b) Output 1 and (c) Output 2, and (d) polarization extinction ratio.

In conclusion, an ADC mode conversion based PBS is proposed for the low-birefringence polarization beam splitting in SiC integrated platforms. We numerically simulate and experimentally demonstrate the device in a 4H-SiCOI chip, with high transmission efficiency, broad operational bandwidth, and large polarization extinction ratio. The measurement results show that it has high transmittance of -0.6 dB and -1.3 dB for the TE and TM polarized light, respectively. The polarization extinction ratio is >32 dB at ∼1560 nm for both polarizations, and is >25 dB and >17 dB in the whole C band, for the TE and TM polarized light, respectively. This work provides an effective solution for low-birefringence polarization beam splitting in SiC integrated platforms with overall high performances, especially high polarization extinction ratio, and paves the way for the polarization diversity applications with SiC photonic integrated circuits.

**Funding.** This work was supported by H2020 FET Open (SiComb, No.899679) and VILLUM FONDEN (VIL50293).

**Disclosures.** The authors declare no conflicts of interest.

**Data availability.** Data underlying the results presented in this paper are not publicly available at this time but may be obtained from the authors upon reasonable request.

## REFERENCES

1. T. Kimoto and J. A. Cooper, *Fundamentals of silicon carbide technology: growth, characterization, devices and applications* (John Wiley & Sons, 2014).
2. H. Okumura, Mrs Bull. **40**, 439 (2015).
3. H. Ou, Y. Ou, A. Argyraki, S. Schimmel, M. Kaiser, P. Wellmann, M. K. Linnarsson, V. Jokubavicius, J. Sun, R. Liljedahl *et al.*, The Eur. Phys. J. B **87**, 1 (2014).
4. M. A. Guidry, D. M. Lukin, K. Y. Yang, R. Trivedi, and J. Vučković, Nat. Photonics **16**, 52 (2022).
5. D. M. Lukin, C. Dory, M. A. Guidry, K. Y. Yang, S. D. Mishra, R. Trivedi, M. Radulaski, S. Sun, D. Vercruysse, G. H. Ahn *et al.*, Nat. Photonics **14**, 330 (2020).
6. S. Castelletto, A. Peruzzo, C. Bonato, B. C. Johnson, M. Radulaski, H. Ou, F. Kaiser, and J. Wrachtrup, ACS Photonics **9**, 1434 (2022).
7. X. Shi, J. Zhang, W. Fan, Y. Lu, N. Peng, K. Rottwitt, and H. Ou, Photonics Res. **10**, A8 (2022).
8. X. Shi, W. Fan, A. K. Hansen, M. Chi, A. Yi, X. Ou, K. Rottwitt, and H. Ou, Adv. Photonics Res. **2**, 2100068 (2021).
9. X. Shi, Y. Lu, N. Peng, K. Rottwitt, and H. Ou, J. Light. Technol. **40**, 7626 (2022).
10. X. Shi, W. Fan, Y. Lu, A. Yi, X. Ou, K. Rottwitt, and H. Ou, "Thermal oxidation assisted chemical mechanical polishing for low-loss 4h-sic integrated photonic devices," in *47th micro and nano engineering conference,* (2021).
11. B.-S. Song, T. Asano, S. Jeon, H. Kim, C. Chen, D. D. Kang, and S. Noda, Optica **6**, 991 (2019).
12. M. A. Guidry, K. Y. Yang, D. M. Lukin, A. Markosyan, J. Yang, M. M. Fejer, and J. Vučković, Optica **7**, 1139 (2020).
13. L. Cai, J. Li, R. Wang, and Q. Li, Photonics Res. **10**, 870 (2022).
14. D. Dai, L. Liu, S. Gao, D.-X. Xu, and S. He, Laser & Photonics Rev. **7**, 303 (2013).
15. C. Li, M. Zhang, H. Xu, Y. Tan, Y. Shi, and D. Dai, PhotoniX **2**, 1 (2021).
16. A. Orieux and E. Diamanti, J. Opt. **18**, 083002 (2016).
17. L. Sansoni, K. H. Luo, C. Eigner, R. Ricken, V. Quiring, H. Herrmann, and C. Silberhorn, npj Quantum Inf. **3**, 1 (2017).
18. S. Wang, M. Zhan, G. Wang, H. Xuan, W. Zhang, C. Liu, C. Xu, Y. Liu, Z. Wei, and X. Chen, Laser & Photonics Rev. **7**, 831 (2013).
19. X. Shi, W. Fan, Y. Lu, A. K. Hansen, M. Chi, A. Yi, X. Ou, K. Rottwitt, and H. Ou, APL Photonics **6**, 076106 (2021).
20. J. Zhang, X. Shi, Z. Zhang, K. Guo, and J. Yang, Opt. Express **30**, 538 (2022).
21. Y. Zhang, Y. He, Q. Zhu, X. Jiang, X. Guo, C. Qiu, and Y. Su, Front. Optoelectron. **11**, 77 (2018).
22. H. Qin, X. Shi, and H. Ou, Nanophotonics **11**, 4909 (2022).
23. X. Chen, X. Shi, P. Qiu, Z. Dai, Y. Yu, X. Song, H. Zhang, M. Chen, Y. Ye, X. Ren *et al.*, Opt. Lett. **47**, 4600 (2022).
24. D. W. Kim, M. H. Lee, Y. Kim, and K. H. Kim, Opt. express **23**, 998 (2015).
25. Y. Kim, M. H. Lee, Y. Kim, and K. H. Kim, Opt. Lett. **43**, 3241 (2018).
26. D. Dai, J. Light. Technol. **30**, 3281 (2012).
27. C. Li and D. Dai, J. Light. Technol. **36**, 2129 (2018).
28. B. Bhandari, C.-S. Im, O. R. Sapkota, and S.-S. Lee, Opt. Lett. **45**, 5974 (2020).
29. Y. Wu, X. Sun, H. Li, C. Lu, Y. Zhang, S. Liu, Y. Zheng, and X. Chen, J. Light. Technol. (2022).
30. K. Mehrabi and A. Zarifkar, JOSA B **36**, 1907 (2019).

## FULL REFERENCES


1. T. Kimoto and J. A. Cooper, *Fundamentals of silicon carbide technology: growth, characterization, devices and applications* (John Wiley & Sons, 2014).
2. H. Okumura, "A roadmap for future wide bandgap semiconductor power electronics," Mrs Bull. **40**, 439–444 (2015).
3. H. Ou, Y. Ou, A. Argyraki, S. Schimmel, M. Kaiser, P. Wellmann, M. K. Linnarsson, V. Jokubavicius, J. Sun, R. Liljedahl *et al.*, "Advances in wide bandgap sic for optoelectronics," The Eur. Phys. J. B **87**, 1–16 (2014).
4. M. A. Guidry, D. M. Lukin, K. Y. Yang, R. Trivedi, and J. Vučković, "Quantum optics of soliton microcombs," Nat. Photonics **16**, 52–58 (2022).
5. D. M. Lukin, C. Dory, M. A. Guidry, K. Y. Yang, S. D. Mishra, R. Trivedi, M. Radulaski, S. Sun, D. Vercruysse, G. H. Ahn *et al.*, "4h-silicon-carbide-on-insulator for integrated quantum and nonlinear photonics," Nat. Photonics **14**, 330–334 (2020).
6. S. Castelletto, A. Peruzzo, C. Bonato, B. C. Johnson, M. Radulaski, H. Ou, F. Kaiser, and J. Wrachtrup, "Silicon carbide photonics bridging quantum technology," ACS Photonics **9**, 1434–1457 (2022).
7. X. Shi, J. Zhang, W. Fan, Y. Lu, N. Peng, K. Rottwitt, and H. Ou, "Compact low-birefringence polarization beam splitter using vertical-dual-slot waveguides in silicon carbide integrated platforms," Photonics Res. **10**, A8–A13 (2022).
8. X. Shi, W. Fan, A. K. Hansen, M. Chi, A. Yi, X. Ou, K. Rottwitt, and H. Ou, "Thermal behaviors and optical parametric oscillation in 4h-silicon carbide integrated platforms," Adv. Photonics Res. **2**, 2100068 (2021).
9. X. Shi, Y. Lu, N. Peng, K. Rottwitt, and H. Ou, "High-performance polarization-independent beam splitters and mzi in silicon carbide integrated platforms for single-photon manipulation," J. Light. Technol. **40**, 7626–7633 (2022).
10. X. Shi, W. Fan, Y. Lu, A. Yi, X. Ou, K. Rottwitt, and H. Ou, "Thermal oxidation assisted chemical mechanical polishing for low-loss 4h-sic integrated photonic devices," in *47th micro and nano engineering conference,* (2021).
11. B.-S. Song, T. Asano, S. Jeon, H. Kim, C. Chen, D. D. Kang, and S. Noda, "Ultrahigh-q photonic crystal nanocavities based on 4h silicon carbide," Optica **6**, 991–995 (2019).
12. M. A. Guidry, K. Y. Yang, D. M. Lukin, A. Markosyan, J. Yang, M. M. Fejer, and J. Vučković, "Optical parametric oscillation in silicon carbide nanophotonics," Optica **7**, 1139–1142 (2020).
13. L. Cai, J. Li, R. Wang, and Q. Li, "Octave-spanning microcomb generation in 4h-silicon-carbide-on-insulator photonics platform," Photonics Res. **10**, 870–876 (2022).
14. D. Dai, L. Liu, S. Gao, D.-X. Xu, and S. He, "Polarization management for silicon photonic integrated circuits," Laser & Photonics Rev. **7**, 303–328 (2013).
15. C. Li, M. Zhang, H. Xu, Y. Tan, Y. Shi, and D. Dai, "Subwavelength silicon photonics for on-chip mode-manipulation," PhotoniX **2**, 1–35 (2021).
16. A. Orieux and E. Diamanti, "Recent advances on integrated quantum communications," J. Opt. **18**, 083002 (2016).
17. L. Sansoni, K. H. Luo, C. Eigner, R. Ricken, V. Quiring, H. Herrmann, and C. Silberhorn, "A two-channel, spectrally degenerate polarization entangled source on chip," npj Quantum Inf. **3**, 1–5 (2017).
18. S. Wang, M. Zhan, G. Wang, H. Xuan, W. Zhang, C. Liu, C. Xu, Y. Liu, Z. Wei, and X. Chen, "4h-sic: a new nonlinear material for midinfrared lasers," Laser & Photonics Rev. **7**, 831–838 (2013).
19. X. Shi, W. Fan, Y. Lu, A. K. Hansen, M. Chi, A. Yi, X. Ou, K. Rottwitt, and H. Ou, "Polarization and spatial mode dependent four-wave mixing in a 4h-silicon carbide microring resonator," APL Photonics **6**, 076106 (2021).
20. J. Zhang, X. Shi, Z. Zhang, K. Guo, and J. Yang, "Ultra-compact, efficient and high-polarization-extinction-ratio polarization beam splitters based on photonic anisotropic metamaterials," Opt. Express **30**, 538–549 (2022).
21. Y. Zhang, Y. He, Q. Zhu, X. Jiang, X. Guo, C. Qiu, and Y. Su, "On-chip silicon polarization and mode handling devices," Front. Optoelectron. **11**, 77–91 (2018).
22. H. Qin, X. Shi, and H. Ou, "Exceptional points at bound states in the continuum in photonic integrated circuits," Nanophotonics **11**, 4909–4917 (2022).
23. X. Chen, X. Shi, P. Qiu, Z. Dai, Y. Yu, X. Song, H. Zhang, M. Chen, Y. Ye, X. Ren *et al.*, "Efficient mode converters and filters using asymmetrical directional couplers with subwavelength gratings," Opt. Lett. **47**, 4600–4603 (2022).
24. D. W. Kim, M. H. Lee, Y. Kim, and K. H. Kim, "Planar-type polarization beam splitter based on a bridged silicon waveguide coupler," Opt. express **23**, 998–1004 (2015).
25. Y. Kim, M. H. Lee, Y. Kim, and K. H. Kim, "High-extinction-ratio directional-coupler-type polarization beam splitter with a bridged silicon wire waveguide," Opt. Lett. **43**, 3241–3244 (2018).
26. D. Dai, "Silicon polarization beam splitter based on an asymmetrical evanescent coupling system with three optical waveguides," J. Light. Technol. **30**, 3281–3287 (2012).
27. C. Li and D. Dai, "Compact polarization beam splitter based on a three-waveguide asymmetric coupler with a 340-nm-thick silicon core layer," J. Light. Technol. **36**, 2129–2134 (2018).
28. B. Bhandari, C.-S. Im, O. R. Sapkota, and S.-S. Lee, "Highly efficient broadband silicon nitride polarization beam splitter incorporating serially cascaded asymmetric directional couplers," Opt. Lett. **45**, 5974–5977 (2020).
29. Y. Wu, X. Sun, H. Li, C. Lu, Y. Zhang, S. Liu, Y. Zheng, and X. Chen, "Lithium niobate thin film polarization beam splitter based on asymmetric directional coupling," J. Light. Technol. (2022).
30. K. Mehrabi and A. Zarifkar, "Ultracompact and broadband asymmetric directional-coupler-based mode division (de) multiplexer," JOSA B **36**, 1907–1913 (2019).